CHINESE OPTICS LETTERS

Vol. 22, No. 1 | January 2024

Watt-level acousto-optically *Q*-switched Pr:YLF laser at 639 nm

Yuchen Xue (薛喻宸), Ruisong Zhang (张瑞松), Zhengdong Dai (戴征东), Zhongyu Wang (王中玉), Huiying Xu (许惠英), and Zhiping Cai (蔡志平)*

Department of Electronic Engineering, School of Electronic Science and Engineering (National Model Microelectronics College), Xiamen University, Xiamen 361005, China

*Corresponding author: zpcai@xmu.edu.cn

Received July 12, 2023 | Accepted September 6, 2023 | Posted Online January 18, 2024

We present a study on a watt-level acousto-optically *Q*-switched Pr:YLF laser at three different repetition rates (10 kHz, 20 kHz, and 50 kHz) for the first time, to the best of our knowledge. The corresponding average output powers and pulse widths were measured to be 1.14 W, 1.2 W, and 1.32 W, and 40 ns, 52 ns, and 80 ns, respectively. A maximum pulse energy of 0.11 mJ was obtained, corresponding to a peak power of up to 2.8 kW at a repetition rate of 10 kHz. The simulated dynamics of a fast *Q*-switched Pr:YLF laser is in agreement with the experiment. The laser's ability to generate stable pulses with high peak power and short pulse width makes it highly desirable for various practical applications, such as laser machining and material processing.

Keywords: red pulsed laser; Pr:YLF; diode pump; acousto-optical *Q* switching.
DOI: 10.3788/COL202422.011402

1. Introduction

High-energy pulsed visible lasers are in high demand in a variety of applications, including, but not limited to, optical microscopy[1], laser displays[2–4], medical applications[5], and laser communications[6]. Moreover, high-power, high-beam-quality red lasers can serve as pumping sources for transparent materials doped with Cr^{3+} and Ho^{3+} ions, such as Cr:LiSAF (Cr^{3+}:$LiSrAlF_6$)[7] and Ho:ZFG (Ho^{3+}-doped zirconium fluoride glass)[8]. In earlier studies, the commonly used technique for generating red laser light was the second-harmonic generation of 1.3 μm fundamental frequency lasers from Nd^{3+}-doped laser crystals using nonlinear optical crystals such as KTP ($KTiOPO_4$) and LBO (LiB_3O_5)[9,10]. This method has been reported by many researchers, and the use of *Q*-switching operations to adjust the pulse width has resulted in output powers mostly in the hundreds of milliwatts range. Up to now, some rare-earth-ion-doped crystals were reported, yielding effective emissions in the red spectral region, such as Pr^{3+}, Dy^{3+}, and Sm^{3+} ions[11]. In recent years, the technology of directly generating red laser light by pumping Pr^{3+}-doped laser materials with a blue laser source has rapidly developed, which has advantages in the aspects of compact structure, high conversion efficiency, and good stability. Pr^{3+}-doped materials have been demonstrated to be one of the most effective solutions for directly generating visible laser radiation due to their large emission cross sections and four-level laser system visible light transitions[12]. With the improvement of the output power of blue laser diodes (LDs) based on GaN, as well as continuous research progress, the output power of the red laser light based on Pr:YLF (Pr^{3+}:$LiYF_4$) has increased from 1.8 mW, which was first reported by Richter *et al.* in 2004[13], to the current maximum of 8.14 W in 2021[14]. Direct red laser generation based on Pr^{3+} doping can also produce effective coherent ultraviolet radiation through simple frequency doubling, offering a straightforward solution for pulsed visible and UV sources, which are required for materials processing[15] and lithography[16].

Pulsed lasers have a wide range of applications that require high pulse energies or peak powers, which cannot be provided by continuous wave lasers. Short pulse lasers can be achieved through passive *Q*-switching or active *Q*-switching techniques. Passive pulse modulation in direct lasers based on Pr^{3+} ions can be realized in a simple and compact system. Passive *Q*-switching uses the nonlinear properties of materials to modulate the laser cavity loss, resulting in a short pulse output. However, the lack of suitable optical modulators in the visible frequency range has hindered the development of the direct generation of visible pulse lasers, i.e., until the emergence of low-dimensional saturable absorbers. Low-dimensional materials have been explored as passive *Q*-switch modulators for Pr:YLF red lasers. These materials possess unique electronic and optical properties that can be harnessed to achieve efficient and compact *Q*-switching. For example, graphene has been demonstrated to be an effective

passive Q-switch modulator due to its large surface area and high nonlinear optical response. In 2019, a 640-nm LD-pumped passively Q-switched graphene/Pr:YLF laser was reported with an average output power of 17 mW and a pulse width of 709 ns[17]. Other low-dimensional materials, such as transition metal dichalcogenides (TMDs)[18,19], black phosphorus (BP)[20], topological insulators (TIs)[21], Au nanorods[22], MXene[23], and CdTe/Cds quantum dots[24], have also been investigated for their potential use in red spectral region Q-switching. In the visible spectral region, the saturation intensity and fluence of low-dimensional saturable absorbers often become extremely high, resulting in an extremely low modulation depth of Q-switching[12]. The average power typically obtained from such Q-switching operation is only on the order of milliwatts in the form of nanosecond pulses. In recent years, some saturable absorbers thought to be in the near-infrared region, such as Cr^{4+}:YAG (Cr^{4+}:$Y_3Al_5O_{12}$) and Co^{2+}:MALO (Co^{2+}:$MgAl_2O_4$), have exhibited saturable absorption properties in the visible region, as determined theoretically and experimentally by Tanaka *et al.*[25–27], and passively Q-switched Pr:YLF lasers in the 640 nm wavelength region were demonstrated. The pulse width was further compressed, and the average output power was enhanced to the watt level. Nevertheless, the drawbacks of the passive Q-switching modulation technique are an uncontrollable pulse repetition rate and a poor pulse energy (typically several microjoules). This presents a significant challenge in achieving reasonably high pulse energies. In contrast, active Q-switching provides greater flexibility in controlling pulse characteristics, including pulse width, repetition rate, and pulse energy. Despite the fact that there are few reports of actively Q-switched lasers in the red spectral region, researchers have been actively studying and developing this topic, making substantial progress. In 2014, Kojou *et al.* demonstrated that high peak power, narrow pulse width Pr:YLF red laser outputs could be achieved using acoustic-optic Q-switching[28]. The highest pulse energy was 27 μJ at 639 nm, and the corresponding pulse width was 17 ns. To the best of our knowledge, the highest peak power was generated by a diode-pumped Pr:YLF laser, reported by Tanaka *et al.*[12], with 640 nm Q-switching by an acousto-optical modulator (AOM) emitting 10 ns pulses at a repetition frequency of 5 kHz with a peak power of 4.5 kW. In 2019, Jin *et al.* achieved single-longitudinal-mode Pr:YLF laser at 639.5 nm by using a combination of an AOM and a Fabry–Perot etalon[29]. The highest pulse energy of 3.94 μJ and the pulse duration of 81.1 ns were obtained at a repetition of 10 kHz. Most recently, in 2021, Yang *et al.* first reported the development of a blue LD-pumped electro-optic (EO) Q-switched Pr:YLF laser, which achieved high-energy visible light output at 639 nm[30]. The shortest pulse duration of 137 ns is obtained at the repetition rate of 100 Hz, corresponding to a single-pulse energy of 260 μJ and peak power of 1.90 kW. Overall, these studies demonstrate the extensive potential of active Q-switching technology for red lasers and have generated considerable research interest in materials science and optical engineering.

In this study, we demonstrated a blue LD-pumped acousto-optically Q-switched Pr:YLF laser at the pulse repetition rate of 10 kHz, 20 kHz, and 50 kHz, respectively, achieving high average output powers and stable pulses at 639 nm. We measured the average output power, pulse width, slope efficiency, and maximum single-pulse energy for each repetition rate, and we also analyzed their variations with absorbed pump power. The maximum single-pulse energies of up to 110 μJ, 60 μJ, and 26 μJ at repetition rates of 10 kHz, 20 kHz, and 50 kHz, respectively, correspond to peak powers of up to 2.8 kW, 1.1 kW, and 0.33 kW, respectively. The laser's output characteristics at different repetition rates have potential for use in a range of applications, including material processing, scientific research, and medical diagnostics.

2. Experimental Setup

Figure 1 shows the photograph [Fig. 1(a)] and the corresponding schematic diagram [Fig. 1(b)] of the InGaN diode laser-pumped Pr:YLF-pulsed laser experimental setup. An a-cut Pr:YLF crystal (3 mm × 3 mm × 15 mm) with a dopant concentration of 0.2% (atomic fraction) was used as the laser gain medium. The crystal's end faces were polished on both sides. To remove the heat produced, the crystal was wrapped in indium foil and placed in a water-cooled copper block. The water-cooling system maintained its temperature at about 16°C with a temperature control precision of 0.1°C. The pump source was a spatially integrated InGaN laser diode module with a maximum output power of 24 W. At the center wavelength of 444 nm, the laser spectrum's full-width at half-maximum (FWHM) is ~2.2 nm. The M^2 factors of the pump beam were measured to be as $M_x^2 = 46.91$ and $M_y^2 = 15.53$ in the horizontal and vertical directions, respectively. A single plane-convex focusing lens with a 90% transmission rate and a focal length of 75 mm was employed to focus the pump beam onto the center of the Pr:YLF crystal. The absorption efficiency of the Pr:YLF crystal for the pump has been measured to be around 47%. A simple linear cavity with two plano-concave mirrors was used. As illustrated in Fig. 2, the input

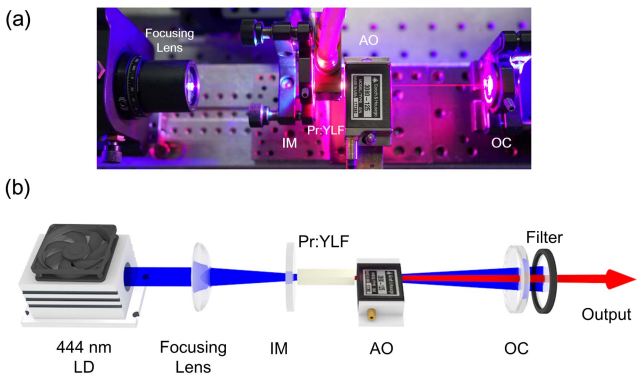

Fig. 1. (a) Photograph of the LD-pumped acousto-optically Q-switched Pr:YLF red laser. (b) Schematic of LD-pumped acousto-optically Q-switched Pr:YLF red laser.

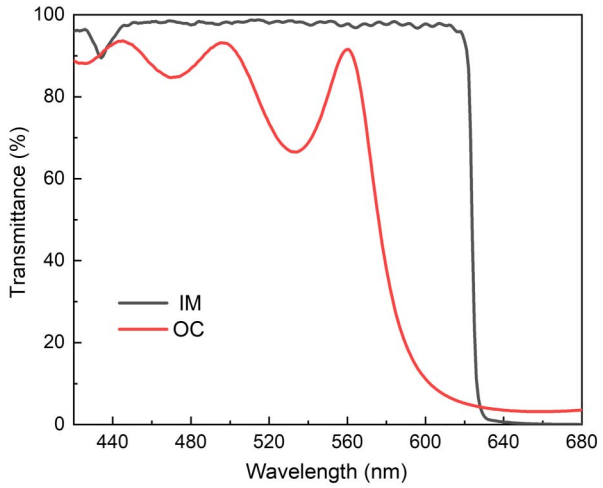

Fig. 2. The coating curves of the IM and the OC.

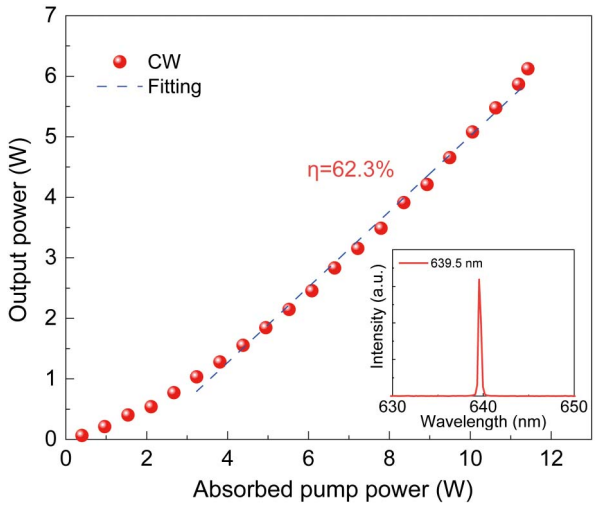

Fig. 3. The continuous-wave (CW) output power versus the absorbed pump power for the wavelength at 639.5 nm.

mirror (IM) was a flat dichroic mirror with a high-transmittance (HT) coating at 444 nm ($T > 96\%$) and a high-reflection (HR) coating at 639 nm ($R > 99\%$). The laser crystal is placed in the cavity immediately near the IM, at the beam waist of the laser mode. The output coupler (OC) was employed with transmissions of 3.5% at 639 nm, and the curve radius was 100 mm, as shown in Fig. 2. By experimentally optimizing the laser system, the effective cavity length of the IM and the OC is obtained as approximately 98 mm. Based on the ABCD matrix, the radius of the laser mode at the center of the laser crystal in the cavity state was calculated to be about 61 μm. A filter was placed behind the OC to block the pump light.

In the experiment, a TeO_2 crystal was purchased from Gooch & Housego and used as the acousto-optical Q-switch crystal (model AOMO3080-125). A digital control driver (model AODR 1080AF-DINA-1.0HCR) was used to drive the acousto-optical crystal, which ensures that the output voltage signal is in real time with the signal generated by the signal generator. When a high-level signal is produced from the signal generator to the crystal driver, a Bragg grating is formed inside the crystal, providing additional loss in the cavity. Conversely, when a low-level signal is output, the Bragg grating disappears, and the additional loss is eliminated, resulting in a high-energy short-pulse laser output. The output power was measured by a laser power meter (Thorlabs, PM100D) and a thermal power sensor head (S442C, 10 mW–50 W). The Q-switched pulses were recorded by a 300-MHz bandwidth digital oscilloscope (Tektronix, TDS3034) and a fast Si free-space amplified photodetector. The output spectra of the Q-switched laser were recorded by the optical spectrum analyzer (Ocean-Optics, HR4000+) with 0.21 nm resolution. The laser beam profile was characterized with a commercial CCD beam analyzer.

3. Results and Discussions

Before inserting the AOM inside the cavity, the continuous-wave (CW) laser was obtained, as shown in Fig. 3. A maximum CW output power of 6.12 W was achieved under the absorbed pump power of 11.4 W, corresponding to a slope efficiency of 62.3%. After optimizing the CW laser cavities, Q-switched lasers have been achieved by inserting the AOM. We successfully operated an AO Q-switched laser at repetition rates of 10 kHz, 20 kHz, and 50 kHz, and we measured the corresponding average output powers to be 1.14 W, 1.2 W, and 1.32 W, respectively. The minimum pulse widths were 40 ns, 52 ns, and 80 ns, respectively. Figure 4 shows the output power and pulse widths as a function of the absorbed pump power for the three repetition rates. The threshold absorbed pump powers were 1.1 W, 960 mW, and 520 mW for the repetition rates of 10 kHz, 20 kHz, and 50 kHz, respectively. The slope efficiencies of the laser were measured to be 11.2%, 11.6%, and 12.4% at repetition rates of 10 kHz, 20 kHz, and 50 kHz, respectively. We observed that the slope efficiency increased with the increasing repetition rate up to 50 kHz.

The slope efficiency typically increases when the repetition rate increases. By increasing the repetition rate, the temporal interval between pulses is reduced, resulting in a decrease in the population inversion loss due to spontaneous radiation transitions. Consequently, this reduction in losses leads to an improvement in the average power output.

The single-pulse energy and peak power could be calculated. Figure 5 illustrates the tendency of the corresponding pulse energy and peak power at a different repetition rate. Under the maximum absorbed pump power of 11.4 W, the maximum single-pulse energy was 110 μJ at 10 kHz, 60 μJ at 20 kHz, and 26 μJ at 50 kHz, respectively, corresponding to the maximum peak powers of 2.8 kW, 1.1 kW, and 0.33 kW. To provide a more accurate description of the operational characteristics of a Pr:YLF-pulsed laser, we simulated the dynamics of a rapidly Q-switched laser using two coupled differential equations[31], where one equation describes the evolution of the photon density and the other describes the evolution of the population inversion density,

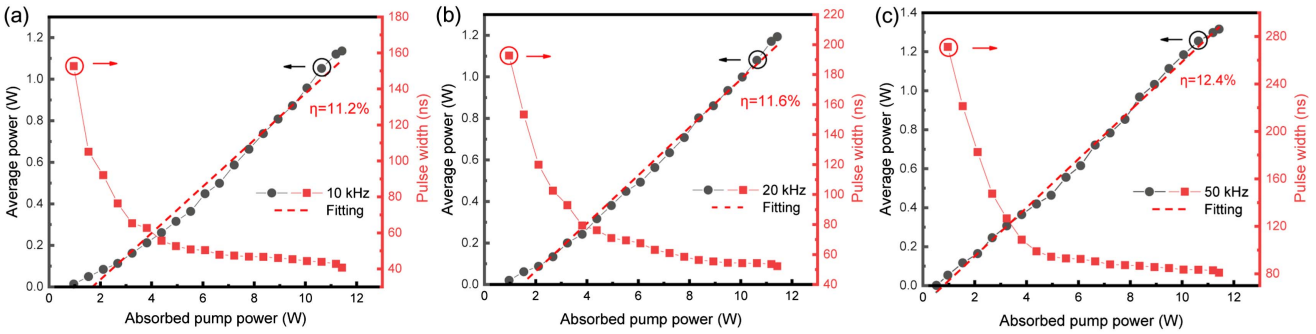

Fig. 4. AO Q-switched average power and pulse width versus the absorbed pump power at different repetition rates of 10 kHz, 20 kHz, and 50 kHz.

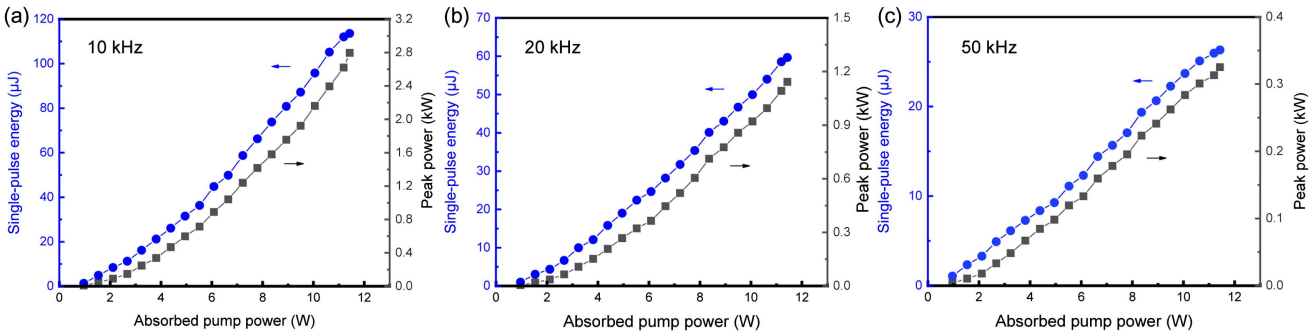

Fig. 5. Single-pulse energy and peak power versus the absorbed pump power at different repetition rates of 10 kHz, 20 kHz, and 50 kHz.

$$\frac{\mathrm{d}\phi}{\mathrm{d}t} = \phi\left(\sigma c n \frac{l_0}{l} - \frac{\varepsilon}{\tau_p}\right), \tag{1}$$

$$\frac{\mathrm{d}n}{\mathrm{d}t} = R_p - \gamma\sigma c n\phi - \frac{n}{\tau}, \tag{2}$$

where ϕ is the photon density, n is the population inversion density, σ is the stimulated emission cross section, and c is the speed of light. τ_p is the photon lifetime; l_0 and l are the laser crystal length and the cavity length, respectively; R_p is the pump rate; γ is the inversion reduction factor; and τ is the lifetime of the excited state. The value of the inversion factor is 1 for a four-level system. The quantity ε in Eq. (1) is the intracavity total losses defined by

$$\varepsilon = -\log(R) + \delta + L, \tag{3}$$

$$\delta = \begin{cases} -\ln(1-\eta) & (0 < t < t_1) \\ 0 & (t_1 < t < t_2) \end{cases}, \tag{4}$$

where R is the output mirror reflectivity, L is the roundtrip dissipative optical loss, δ is the acousto-optically Q-switched modulation loss defined by Eq. (4), and η is the diffraction efficiency. The parameters and their respective values used in the numerical simulation can be found in Table 1. The rate equations were numerically solved using the Runge–Kutta algorithm. As shown in Fig. 6, the simulation results of the population inversion density and the photon density at different repetition frequencies are calculated. Figure 7 demonstrates the typical single-pulse profile and temporal pulse trains, indicating a stable operation of the pulsed laser. The pulse behavior is simulated, and the shape of the pulse is represented by a dashed curve. The M^2 factor was measured to be 1.78 in the x-direction and 1.64 in the y-direction, respectively (see Fig. 8). The measurements were

Table 1. Parameters and Their Values Used in Numerical Simulation.

Symbol	Parameter	Value (or Definition)	Unit
σ	Stimulated emission cross section of the gain medium	2×10^{-19}	cm^2
l_0	Length of the Pr:YLF crystal	15	mm
l	Cavity length	98	mm
τ_p	Photon lifetime	$2l/c$	–
γ	Inversion reduction factor	1	–
τ	Lifetime of the excited state	35	μs
R	Reflectivity of the output mirror	0.965	–
L	Roundtrip dissipative optical loss	0.06	–
η	Diffraction efficiency	0.64	–

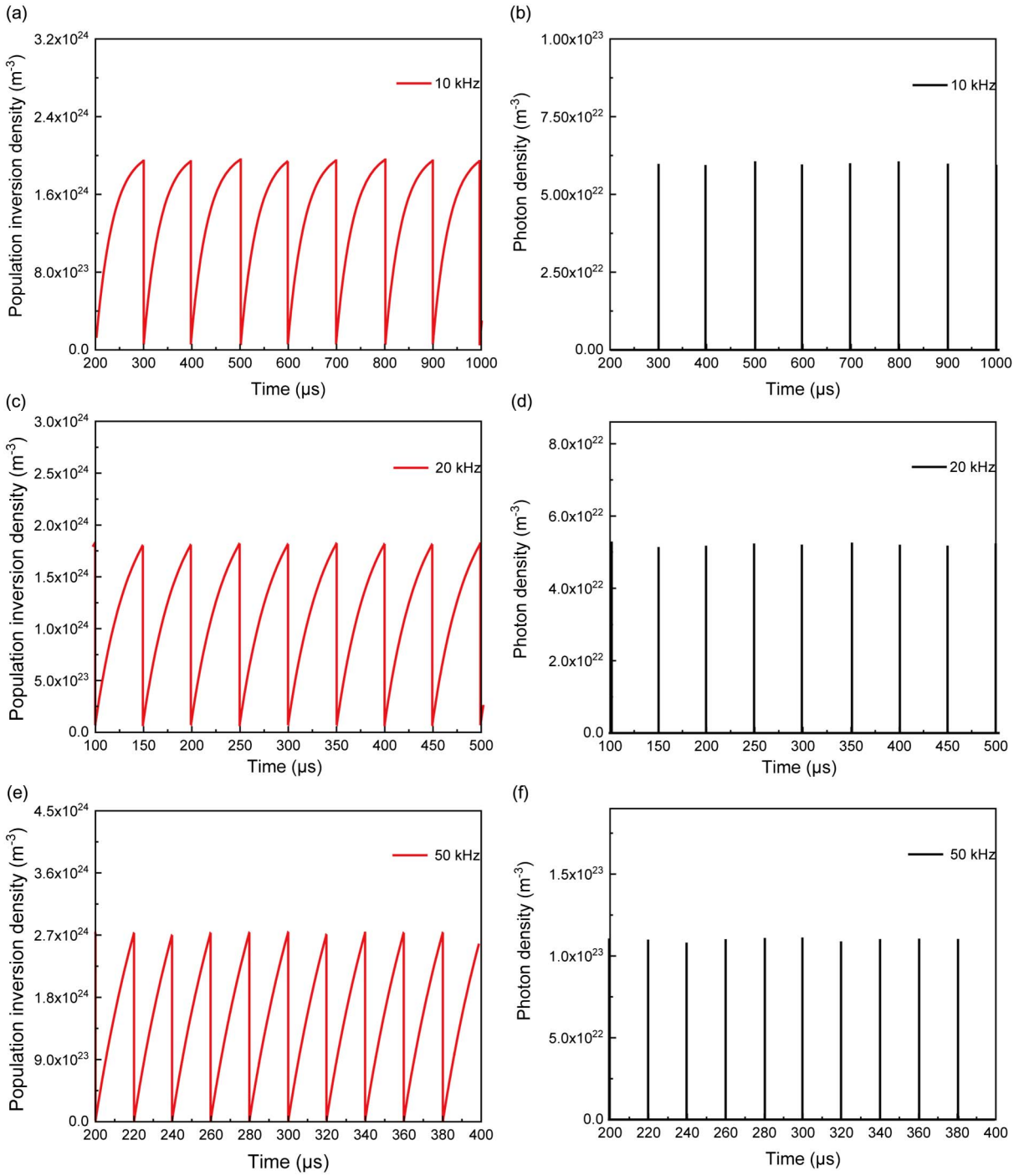

Fig. 6. Numerical simulation results of the population inversion density and the photon density in the cavity at different repetition frequencies.

performed at a repetition rate of 10 kHz and an output power of 1.14 W. To assess the stability of the laser output, we recorded the maximum output power variation of the AO *Q*-switched operation for 1 hour, as shown in the Fig. 9. The fluctuation of the output power (RMS) was measured to be 4.3%, 3.0%, and 1.9%, with different repetition rates of 10 kHz, 20 kHz, and 50 kHz, respectively. These results suggest that the laser output is relatively stable, even under high-power output conditions.

Finally, we compared our results in Table 2 with four other publications that also reported on 639 nm lasers in the Pr:YLF gain medium using active *Q*-switches. We found that our achieved shortest pulse widths are comparable to the previous results in pulse widths. From the experimental and theoretical perspective, our study demonstrates that the blue LD-pumped acousto-optically *Q*-switched Pr:YLF laser has advantages in average output power and single-pulse energy compared to previous studies. To further enhance the laser performance,

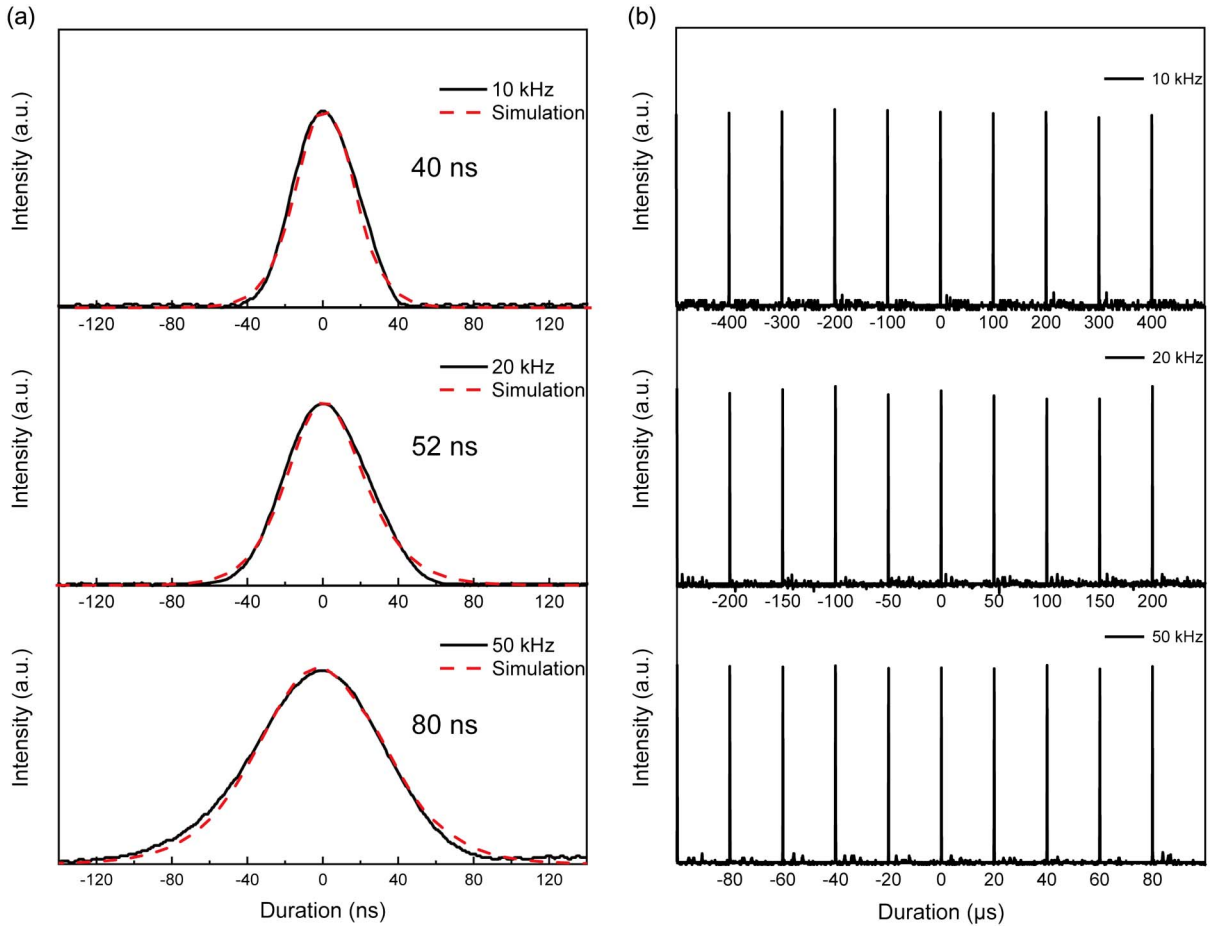

Fig. 7. Characteristics of pulse output at 10 kHz, 20 kHz, and 50 kHz. (a) Single-pulse profiles and (b) typical pulse trains.

we recommend implementing improvements on the AOM. First, adding a water-cooling system to the AOM crystal can help improve its temperature stability and increase its damage threshold. This enhancement enables the laser system to achieve higher output power and peak power while maintaining stability. Second, optimizing the AOM for a higher diffraction efficiency will maximize the light coupling into the resonator, leading to an improved pulse energy. Additionally, increasing the pump power can enhance the population inversion, potentially resulting in shorter pulse durations. Lastly, reducing the

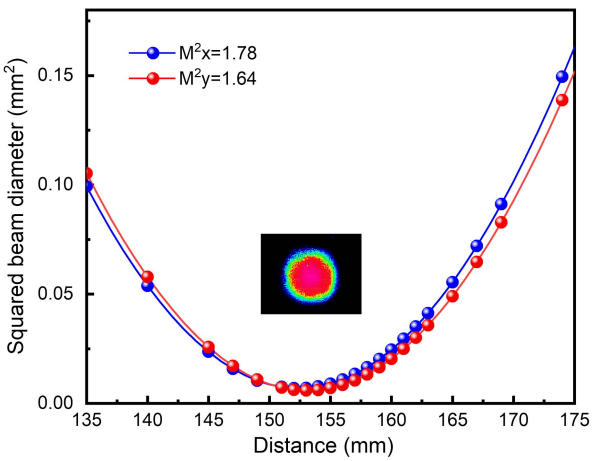

Fig. 8. M^2 factors in the *x*- and *y*-directions. The inset shows the profile of the output captured by a CCD camera.

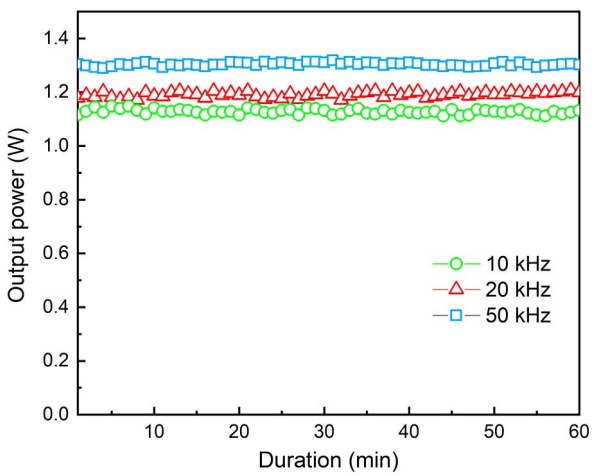

Fig. 9. Stabilities of the AO *Q*-switched output power at different repetition rates.

Table 2. Actively *Q*-Switched Laser Results for 639 nm Based on the Pr:YLF Crystal.

Q-Switch	Average Power (mW)	Peak Power (W)	Pulse Energy (μJ)	Repetition Rate (kHz)	Pulse Width (ns)	Ref.
AO	208	1570	27	7.7	17	[28]
AO	40	48.5	3.94	10	81.1	[29]
AO	280	4500	56	5	10	[12]
EO	26	1898	260	0.1	137	[30]
AO	1136	2796	110	10	40	This work

cavity length remains an effective approach for achieving shorter pulse durations. By incorporating these improvements in the AOM cooling, diffraction efficiency, pumping, and cavity design, we can further enhance the pulse duration and pulse energy of the laser system.

4. Conclusion

In conclusion, we have demonstrated a blue LD-pumped acousto-optically *Q*-switched Pr:YLF laser at three different repetition rates, achieving high average output powers and pulse energies. This study presents a detailed investigation of the output characteristics of a watt-level acousto-optically *Q*-switched Pr:YLF laser operating at 639 nm. The laser showed output characteristics with a minimum pulse width of 40 ns and a maximum peak power of up to 2.8 kW at a repetition rate of 10 kHz. The slope efficiency increased with the increasing repetition rate up to 50 kHz, highlighting the potential for further improvements in laser performance at higher repetition rates. The results of this study provide valuable insights into the optimization of acousto-optically *Q*-switched lasers for practical applications and suggest the potential for their use in various fields, including material processing and spectroscopy.

Acknowledgements

This work was supported by the National Natural Science Foundation of China (No. 61975168). The authors declare that they have no known competing financial interests or personal relationships that could have appeared to influence the work reported in this paper.

References

1. J.-A. Conchello and J. W. Lichtman, "Optical sectioning microscopy," Nat. Methods **2**, 920 (2005).
2. K. V. Chellappan, E. Erden, and H. Urey, "Laser-based displays: a review," Appl. Opt. **49**, F79 (2010).
3. P. M. Smowton, A. A. Belyanin, S. Kawanaka, *et al.*, "USHIO 3.5 W red laser diode for projector light source," Proc. SPIE **10939**, 109391I (2019).
4. K. Yamamoto, "Laser display technologies and their applications," Adv. Opt. Technol. **1**, 483 (2012).
5. P. Shein, C. M. Cilip, G. Quinto, *et al.*, "Selective laser suture lysis with a compact, low-cost, red diode laser," in *30th Annual International Conference of the IEEE Engineering in Medicine & Biology Society* (2008), p. 4358.
6. G. Hu, C. Chen, and Z. Chen, "Free-space optical communication using visible light," J. Zhejiang Univ. Sci. A **8**, 186 (2007).
7. U. Demirbas and I. Baali, "Power and efficiency scaling of diode pumped Cr:LiSAF lasers: 770–1110 nm tuning range and frequency doubling to 387–463 nm," Opt. Lett. **40**, 4615 (2015).
8. S. Ji, S. Liu, X. Lin, *et al.*, "Watt-level visible continuous-wave upconversion fiber lasers toward the "green gap" wavelengths of 535–553 nm," ACS Photonics **8**, 2311 (2021).
9. Z. Y. Li, B. T. Zhang, J. F. Yang, *et al.*, "Diode-pumped simultaneously *Q*-switched and mode-locked Nd:$GdVO_4$/LBO red Laser," Laser Phys. **20**, 761 (2010).
10. H. Q. Zhou, X. L. Bi, S. Q. Zhu, *et al.*, "Multi-wavelength passively *Q*-switched red lasers with Nd^{3+}:YAG/YAG/V^{3+}:YAG/YAG composite crystal," Opt. Quantum Electron. **50**, 56 (2018).
11. C. Kränkel, D.-T. Marzahl, F. Moglia, *et al.*, "Out of the blue: semiconductor laser pumped visible rare-earth doped lasers," Laser Photonics Rev. **10**, 548 (2016).
12. H. Tanaka, S. Kalusniak, M. Badtke, *et al.*, "Visible solid-state lasers based on Pr^{3+} and Tb^{3+}," Prog. Quantum Electron. **84**, 100411 (2022).
13. A. Richter, E. Heumann, E. Osiac, *et al.*, "Diode pumping of a continuous wave Pr^{3+}-doped $LiYF_4$ laser," Opt. Lett. **29**, 2638 (2004).
14. X. Lin, M. Chen, Q. Feng, *et al.*, "LD-pumped high-power CW Pr^{3+}:YLF Laguerre–Gaussian lasers at 639 nm," Opt. Laser Technol. **142**, 107273 (2021).
15. M. R. H. Knowles, A. I. Bell, G. Rutherford, *et al.*, "Applications of high-power visible and UV lasers in manufacturing," Proc. SPIE **3888**, 210 (2000).
16. C. Wagner and N. Harned, "Lithography gets extreme," Nat. Photonics **4**, 24 (2010).
17. Y. Zhang, Y. Yang, L. Zhang, *et al.*, "Watt-level continuous-wave and passively *Q*-switched red lasers pumped by a single blue laser diode," Chin. Opt. Lett. **17**, 071402 (2019).
18. Y. Cheng, H. Yang, B. Xu, *et al.*, "Passive *Q*-switching of a diode-pumped Pr:$LiYF_4$ visible laser using WS_2 as saturable absorber," IEEE Photonics J. **8**, 1501606 (2016).
19. Q. Yang, Y. Cao, X. Liu, *et al.*, "Passive *Q*-switching of Pr:$LiYF_4$ visible laser using SnS_2 as a saturable absorber," Opt. Laser Technol. **112**, 183 (2019).
20. R. Zhang, Y. Zhang, H. Yu, *et al.*, "Broadband black phosphorus optical modulator in the spectral range from visible to mid-infrared," Adv. Opt. Mater. **3**, 1787 (2015).
21. S. Luo, X. Yan, B. Xu, *et al.*, "Few-layer Bi_2Se_3-based passively *Q*-switched Pr:YLF visible lasers," Opt. Commun. **406**, 61 (2018).
22. S. Wang, Y. Zhang, J. Xing, *et al.*, "Nonlinear optical response of Au nanorods for broadband pulse modulation in bulk visible lasers," Appl. Phys. Lett. **107**, 161103 (2015).
23. Q. Yang, F. Zhang, N. Zhang, *et al.*, "Few-layer MXene $Ti_3C_2T_x$ (T = F, O, or OH) saturable absorber for visible bulk laser," Opt. Mater. Express **9**, 1795 (2019).

24. B. Xu, S. Luo, X. Yan, *et al.*, "CdTe/CdS quantum dots: effective saturable absorber for visible lasers," IEEE J. Sel. Top. Quantum Electron. **23**, 1900507 (2017).
25. H. Tanaka, R. Kariyama, K. Iijima, *et al.*, "Saturation of 640-nm absorption in Cr^{4+}:YAG for an InGaN laser diode pumped passively *Q*-switched Pr^{3+}:YLF laser," Opt. Express **23**, 19382 (2015).
26. M. Demesh, D. T. Marzahl, A. Yasukevich, *et al.*, "Passively *Q*-switched Pr:YLF laser with a Co^{2+}:$MgAl_2O_4$ saturable absorber," Opt. Lett. **42**, 4687 (2017).
27. S. Fujita, H. Tanaka, and F. Kannari, "Intracavity second-harmonic pulse generation at 261 and 320 nm with a Pr^{3+}:YLF laser *Q*-switched by a Co^{2+}:$MgAl_2O_4$ spinel saturable absorber," Opt. Express **27**, 38134 (2019).
28. J. Kojou, R. Abe, R. Kariyama, *et al.*, "InGaN diode pumped actively *Q*-switched intracavity frequency doubling Pr:$LiYF_4$ 261 nm laser," Appl. Opt. **53**, 2030 (2014).
29. L. Jin, W. Dai, Y. Yu, *et al.*, "Single longitudinal mode *Q*-switched operation of Pr:YLF laser with pre-lase and Fabry–Perot etalon technology," Opt. Laser Technol. **129**, 106294 (2020).
30. Z. Yang, S. Zaheer Ud Din, P. Wang, *et al.*, "Blue LD-pumped electro-optically *Q*-switched Pr:YLF visible laser with kilowatt-level peak power," Opt. Laser Technol. **148**, 107711 (2022).
31. J. J. Degnan, "Theory of the optimally coupled *Q*-switched laser," IEEE J. Quantum Electron. **25**, 214 (1989).